2020 IEEE/RSJ International Conference on Intelligent Robots and Systems (IROS)
October 25-29, 2020, Las Vegas, NV, USA (Virtual)

# Autonomous Multi-Robot Assembly of Solar Array Modules: Experimental Analysis and Insights

Holly Everson[1], Joshua Moser[2], Amy Quartaro[3], Samantha Glassner[4], and Erik Komendera[5]

***Abstract*— To allow for the construction of large space structures to support future space endeavors, autonomous robotic solutions would serve to reduce cost and risk of human extravehicular activity (EVA). Practicality of autonomous assembly requires both theoretical and algorithmic advances, and hardware experimentation across a spectrum of technological readiness levels. Analysis of hardware experiments provides novel insights not readily apparent in simulations alone, which serves to inform future developments.**

**This paper describes analysis and insights gained from an autonomous assembly experiment consisting of a dexterous manipulator, a gross positioning serial arm, and a 1 degree of freedom (DOF) turntable to facilitate the assembly and deployment of a solar array mockup. This experiment combined state estimation in an uncertain environment with contact-heavy operations such as grasping, self-reconfiguring, joining, and deploying. Insights gained are presented due to their applicability to other field-based manipulation tasks by a team of robots.**

## I. Introduction

Due to the inherently dangerous nature of space, solutions for reducing reliance on human executed tasks are critical to the space industry. The current methods of placing structures into orbit consists of launching completed structures that often perform complex deployment maneuvers increasing mission risk or requiring dangerous EVA tasks such as those performed on the International Space Station. Autonomous robotic operations are seen as a promising solution.

Autonomous robotic in-space assembly (ISA) presents its own challenges in attempting to localize, position, grasp, and manipulate itself, collaborative agents, or assembly components. This presents a need for accurate metrology feedback and structure-aware state estimation, for precise and accurate interactions that are robust to off-nominal conditions. In work initiated at NASA Langley Research Center (LaRC), collaboration of a serial long reach manipulator (LRM) and a precise jigging apparatus has resulted in an assembly methodology for large structures [1]. This placed an emphasis on precise positioning, error mitigation, and the addition of Simultaneous Localization And Mapping (SLAM) in the assembly workspace.

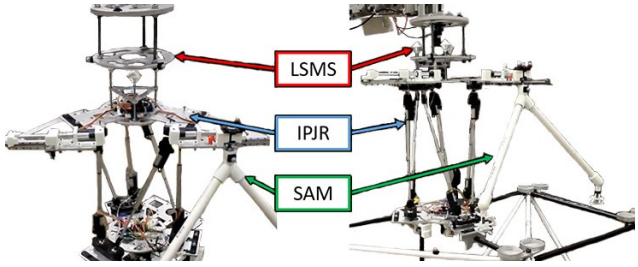


Fig. 1. IPJR Grasping [Left] and Positioning [Right] the SAM

This paper describes in greater depth the results of the solar array assembly experiment seen in Fig. 1 and first described at a high level in [1], and presents insights gained from these observations as informative to future autonomous manipulation, assembly, and deployment scenarios in uncertain environments. This experiment presented a unique opportunity for analysis of the behavior of all workspace objects during the various assembly and deployment steps. Insights gained from this experiment may be useful for other contact-heavy multi-robot manipulation scenarios.

### A. Related Work

Exploration into assembly schemes for ISA often result in a few distinct robotic architectures. Unit assembly and reconfiguration on large structures has been evaluated to utilize structure climbers [2]. JPL also conducted a truss deployment and assembly trial with the use of a single agent, RoboSimian [3]. The concept of combining a LRM and fine positioning jig has also been implemented by LaRC in the Tendon-Actuated Lightweight In-Space MANipulator [4]. Although the following experiment details the assembly of preconstructed truss elements, the concept of collaborative heterogeneous robots can be utilized in a wide range of space assembly tasks [5].

## II. Experimental Architecture

This experiment employed a team of robots, the Lightweight Surface Manipulation System (LSMS) [6] and the Intelligent Precision Jigging Robot (IPJR) [1] in conjunction with a robotic turntable, with supervised autonomy[1]. This system collaboratively worked to position, join, and deploy four solar array modules (SAM) units on a truss. Each object was tracked with a Vicon metrology system [7] during

*This work was supported by the Space Technology Mission Directorate in NASA.

[1]H. Everson is currently a Graduate Research Assistant at the Field and Space Experimental Robotics (FASER) Laboratory, Virginia Tech, Blacksburg, VA hkeverson@vt.edu

[2]J. Moser is currently a Graduate Research Assistant at FASER Laboratory, Virginia Tech, Blacksburg, VA joshnm7@vt.edu

[3]A. Quartaro is currently a Graduate Research Assistant at FASER Laboratory, Tech, Blacksburg, VA aquartaro@vt.edu

[4]S. Glassner is currently a Graduate Research Assistant at FASER Laboratory, Tech, Blacksburg, VA sglassner@vt.edu

[5]E. Komendera is an Assistant Professor of Mechanical Engineering and Director of the FASER Laboratory, Virginia Polytechnic Institute and State University, Blacksburg, VA komendera@vt.edu

[1]In this context, "supervised autonomy" means that a human operator could step in and teleoperate in a contingency. Instances of this are documented in this paper.

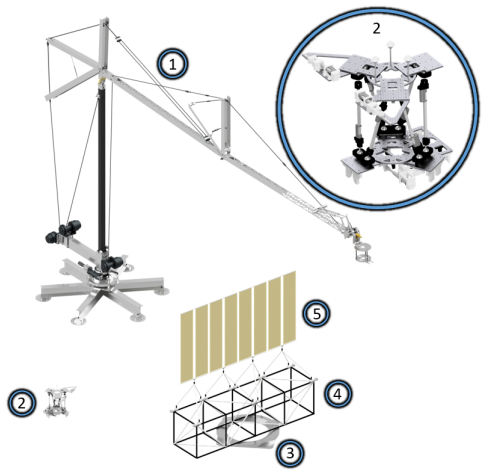


Fig. 2. Workspace depicting the LSMS (1), IPJR (2), turntable (3), truss (4), and SAMs (5) shown in relative size

the experiment with an accuracy of $5mm$ and $0.002rads$, enabling observation of structural and robotic behaviors during contact-heavy operations such as robots grasping each other, grasping the SAMs, and deploying the SAMs. The system implemented a mixed structure-robot state estimate via the Extended Kalman Filter, further explained in [1]. Fig. 2 portrays the workspace state at conclusion of the trial.

The truss utilized was a 4 bay square truss with $1m$ diagonal struts. The truss was mounted on a single DOF turntable, which allowed the LSMS access to all sides of the truss through rotational positioning. Twelve plates were located at nodes atop the truss, corresponding to the 12 legs of the 4 SAMs. Each SAM leg was joined to the plates via hot melt adhesive (HMA), which filled a nominal gap of $1cm$ between the bottom of the leg and the plate. This type of joint enabled full six DOF positioning prior to joining. The SAMs were tripod units that featured two rolled up Mylar sheets attached to a telescoping rod which were deployed via a LSMS end-effector hook, extending the rods.

The LSMS is a tendon actuated robotic arm with an overall boom reach of $7.5m$ [6]. It served as the large envelope gross positioner of the assembly system. It was outfitted with a custom end-effector to allow for the IPJR unit to lock on to it for transport or to become a temporary end-effector. A heat gun was mounted to the end-effector to bond the HMA joints between the truss and the SAMs.

The final robotic element was the IPJR which juxtaposed the LSMS by providing high stiffness and fine precision positioning. The IPJR was a Stewart Platform (SP) with grippers located on the top and bottom plates, allowing grasping of SAMs and the truss. Lifting cones atop the IPJR interlocked into the LSMS end-effector to join the two robots. The SP topology trades off workspace range for high precision and accuracy. Working together, the LSMS and IPJR performed tasks in tandem that neither could do alone, enabling this experiment.

## III. Sequence

The experiment process of assembling and deploying the SAMs is detailed in Fig. 3. Refer to [1] for additional details on tasks were performed. The complete sequence was performed twice, and a modified sequence of a single SAM was performed once, resulting in 9 total SAMs.

**Solar Array Assembly:**

1: **for** Each of four SAMs **do**
2: IPJR grasped SAM at storage
3: LSMS lifted IPJR and transports to assembly site
4: IPJR attached to truss and detached from LSMS
5: IPJR aligned SAM over truss
6: LSMS joined SAM to truss with heat gun
7: LSMS returned IPJR to storage
8: **for** Each of four SAMs **do**
9: LSMS deployed SAMs

Fig. 3. Sequence to assemble a four-module solar array.

## IV. Analysis

Each step depicted in Fig. 3 involved either robots interacting with objects or each other. Measurements of the robots and objects as these interactions started, progressed, and ended were critical to understanding potential sources of error and off-nominal behaviors. The following subsections detail the data, relevant conclusions, and insights. A collection of graphs depict positional errors with respect to relative goal positions, and object motions during tasks with final positions denoted with a small circle. To further clarify values, tables reflecting the graphs have also been included to present basic statistical information. The mean of each assembly step is shown bolded at the bottom of each table.

### A. IPJR Grasped SAM at Storage

This section describes step 2 in Fig. 3, in which the IPJR was located at the storage site then grasped SAMs with its top plate. The values in Table I represent the time the IPJR's top plate took to get to within $3mm$ and $0.052rads$ error per axis with respect to its goal pose in front of each SAM. Fig. 4 shows how the IPJR reached the targeted position over time in the trial. The average final error before performing the grasp was $2.9mm$ and $0.009rads$. In all but one case, the IPJR entered the error margin before autonomously starting the grasp; in one case the operator manually advanced to the grasp step. All nine grasps were successful, with each SAM being captured and shifted to fit within the grasp volume.

### B. SAM Motion During the IPJR Grasp

When the IPJR grasped a SAM, step 2 in Fig. 3, the SAM moved with respect to storage and the IPJR to facilitate the

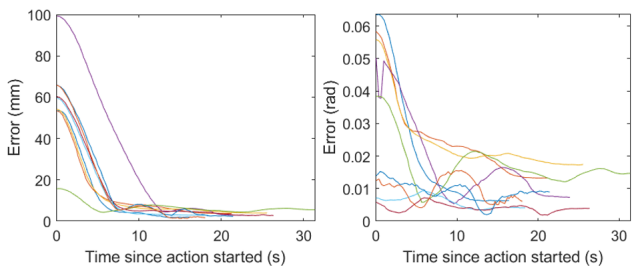


Fig. 4. IPJR Captures SAM (Translational Error[Left] Rotational Error[Right])

TABLE I: ERRORS WHEN IPJR INITIATED SOLAR ARRAY GRASP

| | Time (s) | Trans Errs (mm) | Rot Errs (rad) |
|---|---|---|---|
| Minimum | 16.4 | 1.7 | 0.4E-02 |
| Median | 21.4 | 2.7 | 0.7E-02 |
| Maximum | 31.4 | 5.6 | 1.7E-02 |
| Mean | **22.0** | **2.9** | **0.9E-02** |

grasp. The axes in Fig. 5 show poses relative to the IPJR top frame. Prior to grasping, the IPJR positioned an open gripper to surround the grasp point of a SAM. Due to the IPJR's high stiffness and expected position errors that cannot be completely mitigated, the closing gripper created a closed kinematic chain, thereby inducing stresses more likely to affect the environment than the IPJR. In this environment, friction was the only force keeping the SAMs in place, which passively gave way. As seen in Table II, grasping caused the SAMs to move approximately $20mm$ or more along the X axis, half that range along Y, and a few $mm$ along Z. Although the grippers had a feature to align the SAM and ensure a repeatable pose, the results indicate the final closed pose of a SAM could be quite varied, on the order of 10s of $mm$, informing future designs of a more stable gripper interface. In this experiment, however, the accurate placement of the modules onto the truss was not directly affected by the relative positioning within the grasp, only requiring a reasonably rigid grasp.

### C. LSMS Positioning Over IPJR at Truss and Storage

This section describes a part of step 3 and step 7 in Fig. 3. A key operation that the LSMS was required to repeatedly perform was to maneuver its end-effector close to the IPJR to allow the IPJR to connect with the LSMS within its limited workspace. This operation occurred 46 times over the course of the experiments, starting as far as $1100mm$ away and as close as nearly $10mm$ away as shown in Fig. 6. Depending on the distance, the time required ranged from 17 seconds to 196 seconds reflected in Table III. The average error at the end of each motion was $5.4mm$ and $0.03rads$. The translational error never exceeded $10mm$. The acceptable error margin was $10mm$ on the X and Y axes relative to the global frame, $5mm$ on the Z axis, and $0.088rads$ error on each axis. The rotational error was fairly small despite the 4 DOF LSMS not having a full rotational range of motion. All

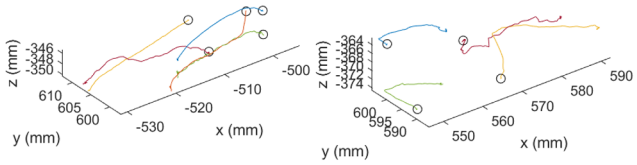


Fig. 5. IPJR Grasps (Left/Right) SAM Motion

TABLE II: MOTION WHEN IPJR GRASPED SAM

| Time (s) | x range (mm) | y range (mm) | z range (mm) |
|---|---|---|---|
| 25.2 | 22.1 | 5.9 | 3.0 |
| 25.2 | 25.9 | 7.0 | 1.5 |
| 25.1 | 19.4 | 2.7 | 2.5 |
| 25.3 | 23.4 | 6.2 | 1.6 |
| 25.2 | 24.1 | 11.1 | 3.4 |
| 25.2 | 16.5 | 3.6 | 3.6 |
| 25.1 | 27.8 | 12.3 | 3.7 |
| 25.0 | 12.6 | 10.3 | 1.8 |
| **25.3** | **25.3** | **2.6** | **4.0** |

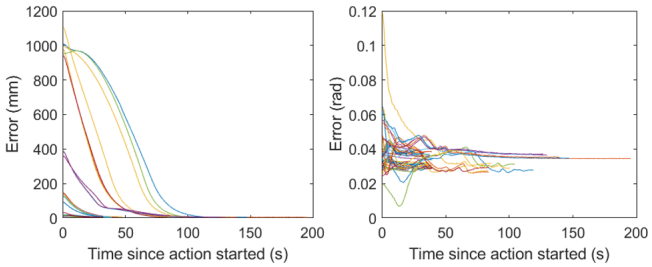


Fig. 6. LSMS Grasps IPJR (Translational Error[Left] Rotational Error[Right])

TABLE III: ERRORS WHEN LSMS GRASPED IPJR

| | Time (s) | Trans Errs (mm) | Rot Errs (rad) |
|---|---|---|---|
| Minimum | 16.8 | 3.8 | 2.6E-02 |
| Median | 38.8 | 5.2 | 3.2E-02 |
| Maximum | 195.5 | 9.6 | 4.0E-02 |
| Mean | **58.4** | **5.4** | **3.3E-02** |

operations were deemed successful as the IPJR joined with the LSMS plate after each motion was completed with no impact. This success shows that a LRM could successfully position itself so that a limited-motion manipulator such at the IPJR could safely and repeatably grasp it to achieve locomotion.

### D. IPJR Grasping the LSMS

This section describes the final part of step 3 and step 7 in Fig. 3, when the IPJR linked to the LSMS. The data shown in Fig. 7 illustrates the error progression of the IPJR's top plate as it moves to capture the LSMS lifting plate. The IPJR penetrated the lifting plate by placing its lifting cones through corresponding holes on the lifting plate, and moved forward to align with the capture slots. The average time required for the IPJR to perform this step, shown in Table IV, was 9.1 seconds with an average error of $2.5mm$ and $0.01rads$. Interesting behavior in which nearly every trajectory underwent a noticeable rebound on the order of $10mm$. This was the result of two processes happening together: the IPJR control law and minor model errors led to an overcorrection step, and the capture process itself led to the IPJR cones interacting with the plate, with each lifting cone settling into the slots at different times, and the plate moving during the operation. Therefore, rebounding errors are an expected result whenever contact occurs.

### E. IPJR Grasping the Truss

This section describes the first part of step 4 in Fig. 3, in which the IPJR grasped the truss while attached to the

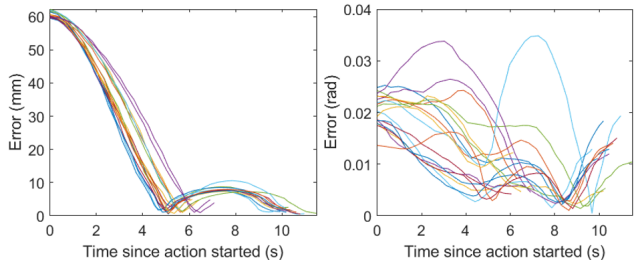


Fig. 7. IPJR Captures LSMS (Translational Error[Left] Rotational Error[Right])

TABLE IV: ERRORS IN IPJR GRASPING LSMS

| | Time (s) | Trans Errs (mm) | Rot Errs (rad) |
|---|---|---|---|
| Minimum | 6.0 | 0.5 | 0.4E-02 |
| Median | 10.2 | 1.7 | 1.2E-02 |
| Maximum | 11.5 | 5.1 | 1.9E02 |
| Mean | **9.1** | **2.5** | **1.0E-02** |

LSMS. As depicted in Fig. 8 the reduction in positional error was significantly reduced below the threshold as the IPJR's bottom plate moved to capture either of the two grasping locations on the truss. In this scenario, the IPJR controller was inverted to drive the bottom plate instead of the top plate. In every case, the LSMS placed the IPJR to $53-63mm$ from the truss, requiring the IPJR to close the remaining error gap. Requiring an average of 23 seconds, the LSMS arrived within an average error of $2mm$ and $0.006rads$ as presented in Table V. Within these margins, the IPJR grasped the truss correctly in all 9 attempts. The error rebound seen in other sequence steps is less pronounced in the translational error, but is visible around 7-10 seconds in rotational error. This can be attributed to small model errors and the control law that result in the trajectory's nonlinear error reduction.

### F. SAM Motion Toward the Goals

The positioning of the SAM by the IPJR, step 5 in Fig. 3, is shown in Fig. 9. The goal positions of the SAMs were located approximately $10mm$ above the truss nodes, such that the HMA simulated welding would mitigate position errors. During this step, the IPJR top plate and the SAM were considered a single object, so the differential kinematics were calculated with the intention of moving the SAMs along straight paths to their goals. The error margins for the SAMs were $5mm$ and $0.05rads$ per axis. The maximum error seen in translation was $6.5mm$, and $0.012rads$ in rotation, as shown in Table VI. The motion profile shows that most trajectories started within $20mm$ of the goal, but two start more than $50mm$ away; this was due to the IPJR top plate having a higher starting point relative to the truss because the LSMS was slightly higher when the disengagement occurred. In most cases the process took 25 seconds or less, but two outliers required 88 and 164 seconds respectively. This was due to controller instability – since

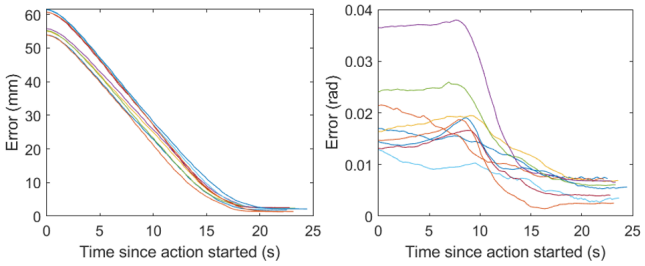


Fig. 8. IPJR Captures Truss (Translational Error [Left] Rotational Error [Right])

TABLE V: ERRORS IN IPJR GRASPING THE TRUSS

| | Time (s) | Trans Errs (mm) | Rot Errs (rad) |
|---|---|---|---|
| Minimum | 22.2 | 1.3 | 0.3E-02 |
| Median | 23.3 | 2.2 | 0.6E-02 |
| Maximum | 24.5 | 2.5 | 0.7E-02 |
| Mean | **23.2** | **2.0** | **0.6E-02** |

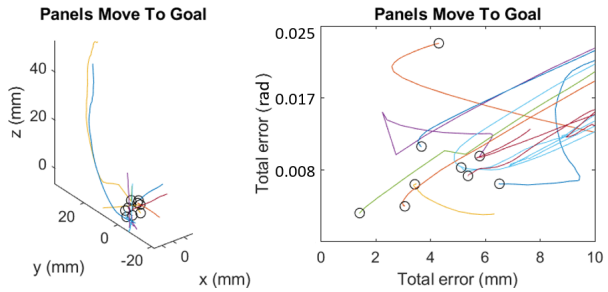


Fig. 9. SAMs Motion to Goal (Isometric [Left] Total Error [Right])

TABLE VI: ERRORS IN MOVING SAMS TO GOAL

| Time (s) | Trans Errs (mm) | Rot Errs (rad) | SAM |
|---|---|---|---|
| 25.7 | 6.5 | 0.7E-02 | P1 |
| 23.5 | 4.3 | 2.4E-2 | P1 |
| 6.3 | 3.4 | 0.7E-02 | P1 |
| 13.7 | 5.8 | 1.0E-02 | P2 |
| 16.8 | 1.4 | 0.4E-02 | P2 |
| 164.2 | 5.1 | 0.9E-02 | P3 |
| 88.5 | 5.4 | 0.8E-02 | P3 |
| 8.2 | 3.7 | 1.2E-02 | P4 |
| 9.1 | 3.1 | 0.4E-02 | P4 |
| **39.6** | **4.3** | **5.4E-01** | |

the SAMs were comparatively far away from the IPJR ball joints, their motion was amplified per unit control. This can be mitigated by using a smaller proportional gain constant for these specific steps, at the cost of increased time. It is important to note that although this data shows all SAMs were placed appropriately prior to joining, this is not the same as saying they remained at their proper position due to deployment settling.

### G. LSMS Moving the Heat Gun to Join SAMs

Step 6 in Fig. 3 required the LSMS to melt the HMA to join the SAMs to the truss. This step required LSMS to achieve a position such that its heat gun could sufficiently heat the HMA attached to each of the legs. Given the size and spread of the hot air, the high accuracy was not required on the X and Y axes ($10mm$), but a small variation in the Z axis could lead to the heat being applied too high or too low with respect to the legs, and that margin was kept to $3mm$. The rotational error margin was kept at $0.175rads$ per axis. 29 trials were performed summed in Table VII: 27 for each of the legs across 9 SAM trials and 2 restarts, including one where a leg was reattached after being dislodged in a collision. The LSMS was able to reach the required rotational accuracy quickly, often converging within 20 seconds, while the total motions required an average of 82 seconds. The translational error was small in most instances, under $10mm$, but on a few occasions the translational error was as high as $46mm$. In these cases, the operator manually advanced the step after deeming that the LSMS had the heat gun properly positioned. Since the LSMS had only four DOF and the turntable had only one, there was insufficient range of motion to completely drive the error down to zero.

### H. SAM Motion After IPJR Release

The motion caused by the release of the joined SAMs, between steps 6 and 7 in Fig. 3, is described in Table VIII. A critical assembly challenge often ignored in autonomous

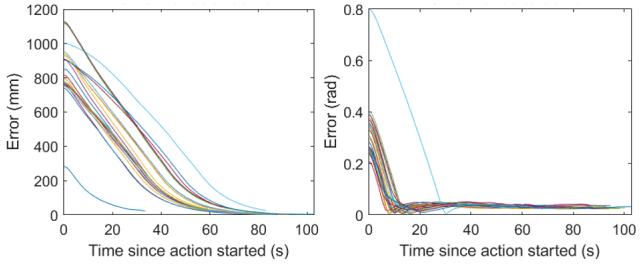


Fig. 10. LSMS Moves Heat Gun to Joint (Translational [Left] Rotational Error[Right])

TABLE VII: ERRORS DURING LSMS POSITIONING HEAT GUN

| | Time (s) | Trans Errs (mm) | Rot Errs (rad) |
|---|---|---|---|
| Minimum | 33.4 | 2.6 | 2.3E-02 |
| Median | 86.6 | 3.4 | 2.9E-02 |
| Maximum | 102.7 | 46.1 | 4.0E-02 |
| Mean | **81.6** | **9.9** | **3.1E-02** |

assembly literature is that the structure itself is flexible and may change over time. Assembly done with strong rigidity assumptions and discretization assumptions (e.g. structures modeled as collections of cubes at integer locations) is prone to failure if flexibility and dynamics are not accounted for. The failures could be as mundane as a joining mistake due to accumulated error growth. To mitigate this, real-time state estimation is necessary to detect and account for such errors. The data here displays a non-hysteretic static changes to the structure: after joining is complete, the IPJR released each SAM, inducing forces on it as it withdrew to link with the LSMS. The SAMs shifted by up to $7mm$ on an axis, but most shifting is on the order of $1mm$. The weight of the SAMs and the induced forces caused each unit to move from its starting position. The effects are caused primarily by three things: the weights of the SAMs compressing the glue (which, for each leg, might not be as strong, leading to an uneven outcome), the effects of the gripper opening, permitting a rebound, and small collisions with the IPJR as it withdrew. Although the release step occurred several minutes after the stated

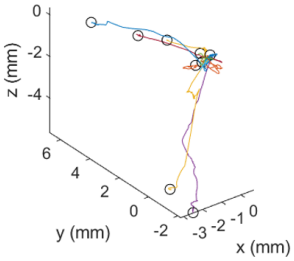


Fig. 11. IPJR Releases SAMs Motion (Isometric)

TABLE VIII: MOTION OF IPJR RELEASING SAMS

| Time (s) | x range (mm) | y range (mm) | z range (mm) |
|---|---|---|---|
| 41.8 | 0.4 | 0.3 | 0.5 |
| 43.7 | 0.4 | 3.4 | 0.8 |
| 45.8 | 0.3 | 1.0 | 0.4 |
| 53.9 | 0.4 | 5.5 | 1.2 |
| 45.1 | 1.0 | 2.5 | 1.2 |
| 47.6 | 2.7 | 2.2 | 5.6 |
| 43.3 | 1.1 | 1.0 | 0.7 |
| 54.3 | 1.0 | 7.2 | 1.1 |
| 43.1 | 3.2 | 1.8 | 4.6 |
| **46.5** | **1.2** | **2.6** | **1.8** |

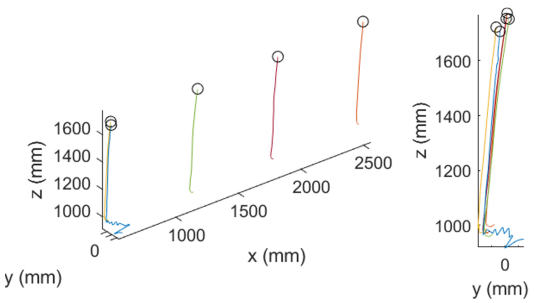


Fig. 12. LSMS SAM Deployment Motion (Isometric [Left] and Left View [Right])

TABLE IX: MOTION OF LSMS DEPLOYING SAMS

| Time (s) | x range (mm) | y range (mm) | z range (mm) |
|---|---|---|---|
| 212.5 | 120.1 | 149.0 | 790.2 |
| 156.3 | 13.8 | 66.9 | 753.8 |
| 164.9 | 11.9 | 93.3 | 793.3 |
| 144.8 | 12.6 | 85.9 | 781.9 |
| 142.7 | 10.2 | 77.7 | 779.8 |
| **152.2** | **12.1** | **81.0** | **777.2** |

curing time of the HMA, it is also possible that the adhesive was still in a heated plastic stage, contributing to the non-hysteresis. The data indicates that predicted settling may not be as straightforward as adding a negative Z component to the joined position. Additional observations are required to formulate a distribution of possible non-hysteretic outcomes for welded joints with and without gravity.

### *I. LSMS Deploying the SAMs*

The SAM deployment, step 9 in Fig. 3, is described here. The motion profiles demonstrate how the LSMS navigated its end-effector while holding onto the SAM's deployable rod. This step was performed only 5 times autonomously shown in Table IX; during the first full autonomous trial, all other steps were performed autonomously, whilst the SAM deployment was trained for the first time and manually driven. The LSMS was commanded to perform a deployment step that moved mostly vertically for each SAM. The deployment of one of the SAMs was used as the template, and the operator did not perform a completely vertical motion, so each SAM was deployed with an average X motion of $12mm$, Y motion of $81mm$, and Z motion of $777mm$. Deployment included 10 intermediate waypoints generated automatically based on the starting and ending poses to prevent model errors from causing the LSMS to place too much strain on the SAMs or cause accidental detachment. These averages exclude the motion for the first autonomous deployment, since that step was used to train the hooking steps preceding deployment (seen in blue on the left view). In all cases, deployment proceeded properly, without loss of contact or broken joints.

### *J. SAM Motion During Deployment*

During deployment, step 9 in Fig. 3, the SAMs moved in place due to the flexible structure. Another critical assembly challenge is induced forces on the structure cause it to flex in ways that could be detrimental to the structure. However, if measured in situ, it could serve as an indicator of structural health. The data in Table X shows how the 5 autonomous deployments affected the positions of each

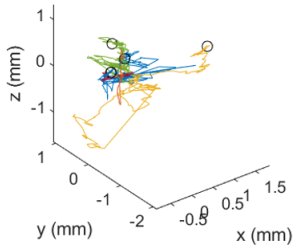


Fig. 13. SAM Deployment Motion (Isometric)

TABLE X: MOTION OF SAMS DURING DEPLOYMENT

| Time (s) | x range (mm) | y range (mm) | z range (mm) |
|---|---|---|---|
| 212.5 | 2.4 | 0.6 | 0.8 |
| 156.3 | 1.5 | 2.6 | 3.0 |
| 164.9 | 0.7 | 1.3 | 1.0 |
| 144.8 | 0.7 | 0.2 | 0.2 |
| 142.7 | 0.7 | 0.8 | 0.6 |
| **164.2** | **1.2** | **1.1** | **1.1** |

of the 5 deployed SAMs during deployment. It is apparent that one SAM moved significantly more than the others, and settled further away during deployment; this could be either an artifact of the LSMS inducing more force through a minor misalignment, or comparatively more flexible adhesive joints. The magnitude of the motion, however, is on the order of $1 - 2mm$, which indicates healthy joints. If any of the joints were not properly made, the SAM would have pivoted around the good joints, and the range of motion would be significantly larger. This motivates an easy-to-implement way to detect if a joint is good: a robot applies a prescribed force and watches how the induced object moves relative to its surroundings. If the motion exceeds a certain threshold, the likelihood of poor joint health will be high.

## V. INSIGHTS

The successful assembly and deployment of a solar array truss by a collaborative robotic team serves to set vital groundwork for the implementation of ISA. Future endeavours would be prudent to note the following:

**Models are always incorrect:** Autonomous trials are more likely to work the less each step requires calibrated knowledge of the robots and objects they are manipulating. Wherever possible, metrology markers and environmental cues should provide corrective feedback, and model errors leading to collisions and induced forces should be assumed. In this work, states and trained goals were based directly on marker locations to mitigate the need for precise knowledge of the robots and objects.

**Uncertain contact-heavy scenarios require passive compliance:** Creating closed kinematic chains in an uncertain environment requires passive compliance, especially if the robotic tool(s) possess high stiffness such as the SP relative to other objects. Compliance is required because repeatability cannot be guaranteed in uncertain environments. Active compliance may be used, but in contact-heavy scenarios, even minuscule control delays could be costly. In this trial, the SAM storage and the LSMS itself were both passively compliant, enabling off-nominal closures to occur safely.

**Objects that look static may not be:** As evidenced in this experiment, throughout the assembly process components will shift and settle in unplanned ways. To ensure proper structural accuracy and allow for the ability to perform corrections, the system must first know that a component has shifted, and to where. Active monitoring will allow a robot to adjust accordingly in the event of a slip or a drop during grasping. If a contact event modifies the environment, active monitoring can relay how and where the contact was made and inform of any changes that resulted from the contact. Such capabilities would allow the agents to reevaluate a changing and uncertain environment with accuracy and precision.

**Environmental assessment with tactile actions:** Active sensing should be used to assess structural health, for example, probing the structure to track its response. This was implicitly done by the active monitoring system during SAM deployment by the LSMS. Implementing this allows for detection and location of damaged members, or determine whether an object is fixed or simply resting. With enough knowledge about the damage case, an autonomous repair capability will follow.

**Autonomous assembly requires more data and better analysis:** Autonomously controlled robots in an uncertain environment require constant data feedback from its environment. To truly eliminate human interaction, these systems must have access to large quantities of information from various sources. This allows robots to interact with their surroundings in a way that is not purely a process of predetermined steps. Through improving sensing and analysis of the data, these autonomous systems will be able to carry out critical tasks such as assembly, inspection, and repair.

## REFERENCES

[1] E. E. Komendera, S. Adhikari, S. Glassner, A. Kishen, and A. Quartaro, "Structure assembly by a heterogeneous team of robots using state estimation, generalized joints, and mobile parallel manipulators," in *Proceedings of the IEEE/RSJ International Conference on Intelligent Robots and Systems*, 2017.

[2] B. Jenett and K. Cheung, "BILL-E: Robotic Platform for Locomotion and Manipulation of Lightweight Space Structures," in *25th AIAA/AHS Adaptive Structures Conference*. American Institute of Aeronautics and Astronautics. [Online]. Available: https://arc.aiaa.org/doi/abs/10.2514/6.2017-1876

[3] S. Karumanchi, K. Edelberg, J. Nash, C. Bergh, R. Smith, B. Emanuel, J. Carlton, J. Koehler, J. Kim, R. Mukherjee *et al.*, "Payload-centric autonomy for in-space robotic assembly of modular space structures," *Journal of Field Robotics*.

[4] E. E. Komendera and J. Dorsey, "Initial Validation of Robotic Operations for In-Space Assembly of a Large Solar Electric Propulsion Transport Vehicle," in *AIAA SPACE and Astronautics Forum and Exposition*. Orlando, FL: American Institute of Aeronautics and Astronautics, Sep. 2017. [Online]. Available: https://arc.aiaa.org/doi/10.2514/6.2017-5248

[5] W. K. Belvin, W. R. Doggett, J. J. Watson, J. T. Dorsey, J. E. Warren, T. C. Jones, E. E. Komendera, T. Mann, and L. M. Bowman, "In-Space Structural Assembly: Applications and Technology," in *3rd AIAA Spacecraft Structures Conference*. San Diego, California, USA: American Institute of Aeronautics and Astronautics, Jan. 2016. [Online]. Available: http://arc.aiaa.org/doi/10.2514/6.2016-2163

[6] J. T. Dorsey, T. C. Jones, W. R. Doggett, J. S. Brady, F. C. Berry, G. G. Ganoe, E. J. Anderson, B. D. King, and C. D. Mercer, "Recent developments in the design, capabilities and autonomous operations of a lightweight surface manipulation system and test bed," in *Proceedings of the AIAA Space Conference*, 2011.

[7] "Vicon homepage," http://www.vicon.com, accessed: 2014 October 22.